Strip track-off and buckling between transport rollers

W.Barrie Fraser and Charlie Macaskill
University of Sydney

Mark McGuinness
Victoria University of Wellington

Aaron Thornton
University of Wollongong

1 Introduction

The problem brought to MISG 2007 by BlueScope Steel is the formation of 'ironed-in' wrinkles in thin steel-sheet products. This is found to occur in a number of environments, but typically is observed in installations where steel sheet is passing over a large number of rollers, some of which drive the sheet and hence provide a tension in the direction of motion. In general, the defects arise sporadically, and only very infrequently. However, they can have a significant cost both because of the loss of product and the difficulty associated with tracking down the cause of the problem. The cause can sometimes be traced to roller misalignment or to metal sheet of non-uniform thickness, for example.

Several different kinds of wrinkles are observed. One type of permanent wrinkle is similar to the folds that are sometimes observed in newspaper printing, which follow a diagonal pattern arising from the edge of a (usually misaligned) roller. The nature of these wrinkles, and the mechanisms leading to their formation, are relatively well-understood in the literature (see e.g. [7] and references therein). This work concentrates on a second kind of wrinkle that occurs more often in practice in cold steel-sheet rolling and that arises in a fundamentally different way. This second kind of wrinkle usually appears as a single thin ridge close to the centre of the sheet and is more prevalent when convex rollers are used to alleviate mistracking (convex rollers have greater radius near the centreline). The wrinkle may have a longitudinal extent of tens of metres but a width of the order of twenty to thirty millimetres and a depth of less than a millimetre. The ridge typically wanders in the lateral direction around the centre of the sheet, as illustrated in Figure 1.

Simple demonstrations with aluminium kitchen foil, as in Figure 2, show that a thin metal sheet under longitudinal tension and with clamped ends will certainly support small amplitude elastic wrinkles, elongated in the longitudinal direction, giving an appearance like corrugated roofing steel. However, these wrinkles are not permanent and disappear when the applied tension is reduced. Moreover, such wrinkles, discussed in the literature in a number of contexts, [2, 6, 13, 14, 15], clearly require a locally compressive field.

This group was asked to model the formation of longitudinal wrinkles in steel moving under tension between rollers, and in particular:

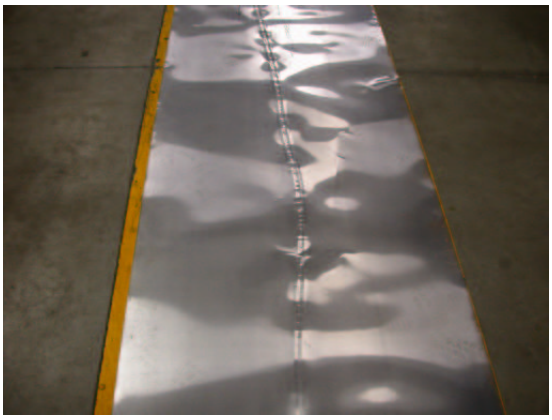

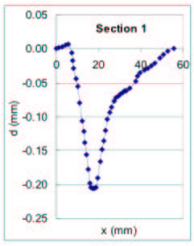

Figure 1: Example of a longitudinal wrinkle in flat steel, and a cross section illustrating typical changes in thickness across the wrinkle.

1. to understand the mechanisms giving rise to local cross-plate compression, which is a necessary prerequisite for initial wrinkle formation;

2. to develop a theoretical model describing the vertical deflection due to this compression;

3. to determine the mechanisms for the *iron-on* process as a wrinkle approaches a roller.

We use von Kármán's weakly nonlinear equations for the moderately large deflection of thin, initially flat, elastic plates to address the problem of how wrinkles are initiated under sufficiently high longitudinal tension applied to the ends of a plate. If, in addition, the assumption is made that the vertical deflections are very small, then the equations decouple and the in-plane stresses in the plate obey a (linear) biharmonic equation, so that the stresses can be determined without reference to any knowledge of the vertical deflections. The remaining problem is then to determine the nature of the boundary conditions. The lateral boundaries of the plate are clearly stress-free. The boundary conditions at the ends (at the rollers) are more problematic. Here we make the simplifying approximation that the plate is clamped against movement in both the longitudinal and lateral directions. The underlying assumption is that the friction in the along-roller direction, due to the pressure imposed by the roller nip, is sufficient to prevent any lateral motion there.

Under these conditions, numerical solutions of the biharmonic equation for the stresses reveal a local cross-plate compressive stress quite close to each of the rollers. Furthermore, if a roller is convex, giving rise to a maximum in both the *longitudinal* and *cross-plate* tensions at the centreline at the roller location, then there is a corresponding maximum in *cross-plate compression* at the centreline some distance from the roller. Thus proper consideration of the boundary conditions provides an explanation for point 1 above.

The above findings explain how a maximum elastic deformation will be found near to the roller location and at the centreline of the plate. However, in order to see a permanent distortion of the plate, the elastic stresses must exceed the plastic yield limit, hence 'setting in' the distortion. For this to happen the local radius of curvature of the distortion must be quite small: for thin steel sheet we estimate that the vertical deflection divided by the lateral wavelength must be greater than about 1/20. In order to determine this ratio, the full

Figure 2: Experiments producing wrinkles in tin foil by stretching lengthwise.

nonlinear von Kármán equations must be solved iteratively in order to determine the vertical deflection over the plate, in particular at the location of maximum compression.

A further question to be addressed is that although initiation of the ridge-like distortion is apparently random (e.g. a roller is slightly out of alignment), once a distortion is initiated it tends to continue over long lengths of material. One possible explanation for this is that a local ridge in the plate when reaching the roller will lead to a modified tension at the roller that in turn influences the compression upstream: this proposed effect can only be explored with careful solution of the full governing equations with small perturbations in the roller boundary conditions. This exploration is beyond the scope of the current work.

In sections 2, 3 and 4 we solve von Kármán's equations for moderately large deflections of thin elastic plates. Dynamic effects due to the motion of the plate and elastic (bending and in-plane) waves, and transverse waves due to the tension will all be ignored. This assumption is discussed more fully in section 6. In section 5 the use of energy methods (see [2]) is discussed and compared with our results. Finally, in section 7, we describe a mechanism explaining how these wrinkles may be ironed in due to plastic deformation when a wrinkled section of the plate moves over an intermediate, single, freely rotating roller.

2 Mathematical formulation

It is observed that when long rectangular plates are subject to large tension in the length-wise direction that lateral wrinkling of the plate occurs with the wrinkles aligned in the length-wise direction. Since the velocities of in-plane and transverse elastic waves are large compared with the transport velocity, we ignore the dynamic effects here.

We model this problem using the weakly nonlinear von Kármán equations. Let the plate have uniform thickness h and width $2d$, and let the distance between the rollers be 2ℓ. We take

Cartesian axes (x, y, z) so that x, y lie in the plane of the middle surface of the undeformed plate with x coincident with the central axis of the strip, and z in the direction perpendicular to this plane, as illustrated in Figure 3. Let the displacement components of the deformed middle surface in the x, y, z directions respectively be given by u, v, w. We use the equations

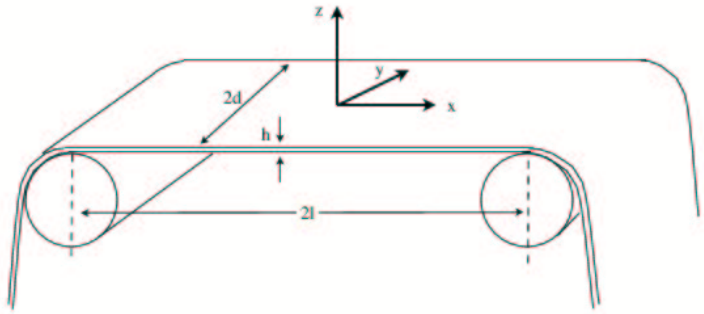

Figure 3: Sketch of dimensions and axes for modelling strip deformation across rollers.

in the form given in [11] (p. 415) (see also [8]). The stress function compatibility equation, and the transverse equilibrium equation, normal to the middle surface, are respectively

$$\nabla^4 \phi = -\frac{Eh}{2} L(w, w), \quad D\nabla^4 w = L(\phi, w), \tag{1}$$

where E is Young's modulus, ν is Poisson's ratio and the plate bending stiffness is given by $D = Eh^3/12(1-\nu^2)$.

The operators ∇ and L are defined as follows:

$$\nabla^4 \equiv \left(\frac{\partial^2}{\partial x^2} + \frac{\partial^2}{\partial y^2} \right)^2, \quad L(A, B) = A_{xx} B_{yy} - 2A_{xy} B_{xy} + A_{yy} B_{xx} \ ,$$

and the in-plane stress resultants are given in terms of the stress function ϕ by

$$N_{xx} = \frac{\partial^2 \phi}{\partial y^2} = \phi_{yy} \ , \quad N_{yy} = \frac{\partial^2 \phi}{\partial x^2} = \phi_{xx} \ , \quad N_{xy} = -\frac{\partial^2 \phi}{\partial x \partial y} = -\phi_{xy} \ , \tag{2}$$

where N_{xx}, N_{yy} and N_{xy} are forces per unit length. The middle surface strain/displacement equations and in-plane stress resultant constitutive equations are as follows:

$$\begin{aligned} e_{xx} &= \frac{\partial u}{\partial x} + \frac{1}{2}\left(\frac{\partial w}{\partial x}\right)^2 = \frac{1}{Eh}(N_{xx} - \nu N_{yy}) \ , \\ e_{yy} &= \frac{\partial v}{\partial y} + \frac{1}{2}\left(\frac{\partial w}{\partial y}\right)^2 = \frac{1}{Eh}(N_{yy} - \nu N_{xx}) \ , \\ e_{xy} = e_{yx} &= \frac{1}{2}\left(\frac{\partial u}{\partial y} + \frac{\partial v}{\partial x} + \frac{\partial w}{\partial x}\frac{\partial w}{\partial y}\right) = \frac{(1+\nu)}{Eh} N_{xy} \ , \end{aligned} \tag{3}$$

where e_{xx}, e_{xy} and e_{yy} are the strains.

2.1 Boundary conditions

Equation (1) must be solved subject to boundary conditions, appropriate to the problem, which will now be derived. The lateral edges at $y = \pm d$ are assumed to be free from stress and moment. The derivation of the 'free edge' conditions for plate theory, which is due to Kirchhoff, is given in [11] (p. 83). The conditions are that the normal component of the bending moment and the effective shear must be zero on the free edges, and the in-plane stress resultant must also vanish there. In this case the first two boundary conditions are

$$\left.\begin{aligned} \frac{\partial^2 w}{\partial y^2} + \nu \frac{\partial^2 w}{\partial x^2} &= 0 \\ \frac{\partial^3 w}{\partial y^3} + (2-\nu)\frac{\partial^3 w}{\partial x^2 \partial y} &= 0 \end{aligned}\right\} \quad \text{at} \quad y = \pm d, \tag{4}$$

and the zero in-plane tension on the boundary is

$$N_{yy} = \phi_{xx} = 0, \quad \text{and} \quad N_{xy} = -\phi_{xy} = 0\,. \quad \text{at} \quad y = \pm d. \tag{5}$$

Here we assume that the plate is fully clamped at the rollers at $x = \pm \ell$, which is the simplest possible boundary condition for perfectly aligned rollers. This implies the following conditions on the strains and displacements:

$$\left.\begin{aligned} w = \frac{\partial w}{\partial x} &= 0, \quad v = \frac{\partial v}{\partial y} = 0 \\ N_{xx} = \frac{\partial^2 \phi}{\partial y^2} &= N_0 f(y) \end{aligned}\right\} \quad \text{on} \quad x = \pm \ell \tag{6}$$

where $f(y)$ is a shape function with unit order of magnitude. To obtain the other boundary condition at the rollers, the above boundary conditions are used to evaluate the strain e_{yy} in equations (3) and we obtain $e_{yy} = 0 = (N_{yy} - \nu N_{xx})/Eh$ on $x = \pm \ell$ so that

$$N_{yy} = \phi_{xx} = \nu N_0 f(y) \quad \text{on} \quad x = \pm \ell\,, \tag{7}$$

where N_0 is the magnitude of the tension applied to the plate between the rollers. Here we take $f(y) = 1 - y^2$, as is appropriate for convex rollers. This completes the formulation of the problem.

2.2 Dimensionless equations

In order to construct a sensible non-dimensionalisation for these equations we note that the order of magnitude of the strain in the x-direction caused by the tension N_0 is N_0/Eh so that the order of magnitude of the in-plane displacements u, v will have a maximum value of $(N_0/Eh)d$. From the strain/displacement equations (2) we note that the contribution of the lateral displacement w to the middle-surface strain suggests that to be significant the order of magnitude of w will need to be $(\sqrt{N_0/Eh})d$. With this in mind we introduce the following dimensionless (barred) variables:

$$\begin{gathered} (\bar{x}, \bar{y}) = \frac{(x, y)}{d}, \quad (\bar{u}, \bar{v}) = \frac{(u, v)}{(N_0/Eh)d}, \quad \bar{w} = \frac{w}{(\sqrt{N_0/Eh})d}, \\ \bar{\ell} = \frac{\ell}{d}, \quad \bar{N}_{\alpha\beta} = \frac{N_{\alpha\beta}}{N_0}, \quad \bar{\phi} = \frac{\phi}{N_0 d^2}. \end{gathered} \tag{8}$$

Note that as all quantities will be dimensionless from now on the barred notation will be dropped.

The dimensionless forms of equation (1) are

$$\begin{aligned} \nabla^4\phi &= -\frac{1}{2}L(w,w), \quad \nabla^4 w = \lambda L(\phi, w), \\ \text{where} \qquad & \lambda = \frac{12(1-\nu^2)N_0 d^2}{Eh^3} \end{aligned} \tag{9}$$

is the non-dimensional tension applied to the plate.

Equations (3) become

$$\begin{aligned} e_{xx} &= \frac{\partial u}{\partial x} + \frac{1}{2}\left(\frac{\partial w}{\partial x}\right)^2 = \phi_{yy} - \nu\phi_{xx}\ , \\ e_{yy} &= \frac{\partial v}{\partial y} + \frac{1}{2}\left(\frac{\partial w}{\partial y}\right)^2 = \phi_{xx} - \nu\phi_{yy}\ , \\ e_{xy} = e_{yx} &= \frac{1}{2}\left(\frac{\partial u}{\partial y} + \frac{\partial v}{\partial x} + \frac{\partial w}{\partial x}\frac{\partial w}{\partial y}\right) = -(1+\nu)\phi_{xy}\ . \end{aligned} \tag{10}$$

The dimensionless boundary conditions corresponding to (4) to (7) are obtained by setting $N_0 = 1$ in these equations.

3 Solution procedure

For moderate levels of tension N_0 the plate will remain flat. The question is: at what level of tension do wrinkles appear? Thus we solve the above system as a bifurcation problem for the load parameter λ using an iterative numerical solution as follows.

Step one is to solve the following problem for $\phi^{(0)}$ when $w^{(0)} = 0$:

$$\nabla^4\phi^{(0)} = 0, \tag{11}$$

subject to the boundary conditions (5) and (7) (with $N_0 = 1$).

Now solve the following eigenvalue problem to find the first approximation to the critical load parameter $\lambda^{(1)}$ and the wrinkle pattern $w^{(1)}$,

$$\nabla^4 w^{(1)} = \lambda^{(1)} L(\phi^{(0)}, w^{(1)}), \tag{12}$$

subject to boundary conditions (4) and (6) (with $N_0 = 1$). Let the eigenfunction be normalised to some (small) value $\max|w^{(1)}(x,y)| = \varepsilon$. This solution can now be used to initiate the following iterative procedure.

At the nth iteration $\phi^{(n)}, w^{(n+1)}$ satisfy the equations

$$\nabla^4\phi^{(n)} = -\frac{1}{2}L(w^{(n)}, w^{(n)}), \tag{13}$$

subject to boundary conditions (5) and (7) and

$$\nabla^4 w^{(n+1)} = \lambda^{(n+1)} L(\phi^{(n)}, w^{(n+1)}), \tag{14}$$

subject to boundary conditions (4) and (6). This process is repeated for $n = 1, 2, 3, \cdots$, until convergence is achieved. The iteration is now repeated for a new value of ε and in this way the bifurcation diagram showing λ as a function of ε can be constructed.

Equations (13) and (14) are solved by discretising using second order finite differences. With $x_i = i\Delta$, $i = 1 \ldots m_x$, $y_j = j\Delta$, $j = 1, \ldots m_y$, $\Delta = 2/(m_y - 1)$, (so that $m_x/m_y = \ell$) write $\phi_{i,j}^{(n)} = \phi^{(n)}(x_i, y_j)$ and $w_{i,j}^{(n)} = w^{(n)}(x_i, y_j)$ and then the discrete form of (13) is

$$D_\phi \, \mathbf{\Phi}^{(n)} = -\frac{1}{2}\mathbf{r}^{(n)}. \tag{15}$$

Here D_ϕ is the $m_x m_y \times m_x m_y$ (sparse) banded matrix arising from the finite difference implementation of the biharmonic operator ∇^4, $\mathbf{\Phi}^{(n)} \equiv \phi_{i,j}^{(n)}$ is the vector of unknown values of the stress function ϕ at iteration n and $\mathbf{r}^{(n)}$ is the vector corresponding to the finite difference form of the term $-L(w^{(n)}, w^{(n)})/2$. (Note that at each iteration n, $w^{(n)}$ is known, with $w^{(0)} = 0$.) The boundary conditions on ϕ, equations (5) and (7), are also discretised to second order, with guard points added on each edge of the rectangular domain to allow straightforward treatment of the condition $\phi_{xy} = 0$ on $y = \pm d$. Similarly the discrete form of (14) is

$$D_w \, \mathbf{w}^{(n+1)} = \lambda B \, \mathbf{w}^{(n+1)}, \tag{16}$$

where $\mathbf{w}^{(n+1)} \equiv w_{i,j}^{(n+1)}$ is the vector of the unknown values of the vertical deformation w at iteration $n+1$, and where B is the sparse banded matrix for the discrete form of the operator on the right hand side of (14), i.e.

$$B \equiv \phi_{xx}^{(n)} \frac{\partial^2}{\partial y^2} - 2\phi_{xy}^{(n)} \frac{\partial^2}{\partial x \partial y} + \phi_{yy}^{(n)} \frac{\partial^2}{\partial x^2} \tag{17}$$

with $\phi^{(n)}$ known for each n from (15). The sparse banded matrix D_w represents the biharmonic operator ∇^4 but differs from D_ϕ in that the boundary conditions (4) for w are included rather than those for ϕ, again with the use of guard points. Equations (15) and (16) are solved using MATLAB. At each iteration, the linear problem for $\mathbf{\Phi}^{(n)}$, equation (15) is inverted. When $n = 0$, the right hand side $\mathbf{r}$ is zero except at boundary points. Once $\mathbf{\Phi}^{(n)}$ is known, the eigenvalue problem (16) must be solved. In practice, it was found that rewriting (16) as

$$B \, \mathbf{w}^{(n+1)} = \frac{1}{\lambda} D_w \, \mathbf{w}^{(n+1)} = \hat{\lambda} D_w \, \mathbf{w}^{(n+1)}, \tag{18}$$

and solving for $\hat{\lambda} = 1/\lambda$ was more satisfactory than attempting to solve (16) directly. Equation (18) is a generalized eigenvalue problem and B is *not* positive definite symmetric. Therefore the inbuilt MATLAB sparse eigenvalue solver `eigs.m` cannot be used. However, the routine `ahbeigs.m` ([1]) solves this more general problem and was used for all results presented here. The four modes with smallest positive eigenvalue λ are those considered in the remainder of this paper; these correspond to the largest positive values of $\hat{\lambda}$. (Modes with positive values of λ are those that arise when a plate is subject to longitudinal stretching; longitudinal compression gives negative values of λ and buckling modes.) The iteration process must be carried through to convergence for each value of the maximum absolute vertical deformation ε and for each of the four eigenvalues corresponding to that value of ε. The convergence criterion used was that the absolute relative change in the eigenvalue was less than 10^{-6}. No difficulties were obtained with lack of convergence in any of the cases treated here. However,

we note that more sophisticated methods for the determination of the eigenvalues have been used successfully for the related buckling problem, where the plate is subjected to longitudinal compression (see, for example, [3, 5, 9]). In particular, the numerical results of [3] are consistent with the analytical results of [10]. These more advanced numerical techniques should also work for the plate under tension problem considered in the present work. As all calculations use equal increments in x and y, cases where the aspect ratio $\alpha = \ell/d$ are large require significantly more computational resources. In order to retain reasonable levels of accuracy in estimating the eigenvalues, only values of α less than or equal to three are considered here. Explicitly using odd/even symmetries for particular modes in both x- and y-directions and moving to a fully-compiled language will allow the range of computation to be extended.

4 Results

In this section we present results for the force distribution, eigenmodes of deformation and corresponding eigenvalues for two specific cases, the first a square plate where the aspect ratio $\alpha = 1$ and the second an elongated plate, where $\alpha = 3$, with the second case having more relevance to the BlueScope steel problem.

In Figure 4, surface plots of $N_{yy} = \phi_{xx}$ are shown for the case of zero vertical deformation, i.e. corresponding to the solution of $\nabla^4 \phi = 0$. In Figure 4(a), where $\alpha = 1$, we see a significant region in the centre of the plate where N_{yy} is negative, corresponding to a region of compression. In Figure 4(b), where α is much larger, the region of compression has split into two symmetric regions near to the ends $x = \pm\ell$, i.e. close to the rollers. This localisation of the compressive forces presumably remains for larger values of α. These results confirm the presence of a significant compressive force just upstream from the downstream roller, as proposed at MISG2007.

Figures 5 and 6 show the first four eigenmodes of deformation at iteration $n = 0$, for $\alpha = 1$ and $\alpha = 3$ respectively. These correspond to the linearised approximation where the amplitude of $w(x, y)$ is not known or equivalently the case of vanishing amplitude, i.e. $\varepsilon = 0$. These modes are those with the four smallest positive values λ, which by (9) corresponds to those that first arise under longitudinal tension N_0 applied at the ends of the plate. In Figure 5, for the square plate all modes are even in x, with the first and third modes odd in y and the second and fourth even in y. The third and fourth modes have significantly larger eigenvalues (corresponding physically to greater tension N_0) but with half the transverse wavelength. Comparing these results with Figure 6, we see corresponding modes for the elongated plate, but with deformation more localised in the vicinity of the rollers, as expected from the stress distribution. Furthermore, modes 3 and 4 are *odd* in x for the rectangular plate, rather than even. This occurs because the ordering of the higher order modes changes as α is varied between 1 and 3.

We now consider solutions of the full nonlinear system, as discretised in equations (15) and (16). It turns out that the structure of the eigenmodes of deformation is fairly insensitive to the magnitude of deformation ε, at least for the moderate amplitudes considered here, so that the results displayed in Figure 5 and 6 can be viewed as holding across all values of ε. Thus we present here only the variation of the eigenvalues λ with ε for different resolutions as determined by the number of mesh-points m_x, m_y in the x- and y-directions respectively. In all cases no more than 6 iterations were required to obtain convergence for a given value of

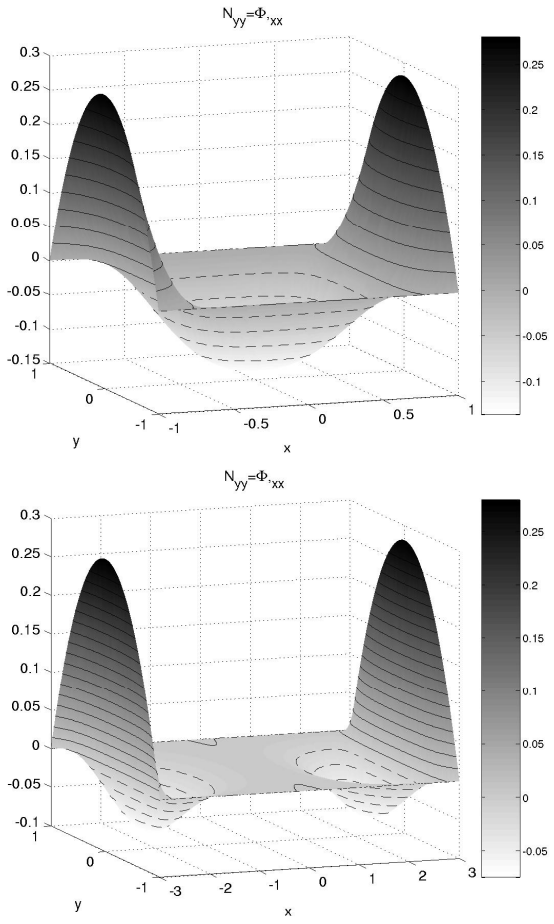

Figure 4: Transverse force per unit length N_{yy} for zero vertical deformation in the cases (a)(*above*) $\alpha = 1$ and (b)(*below*) $\alpha = 3$.

ε. Converged results from a previous value of ε, e.g. $\varepsilon = 0.5$ are used as the starting iteration for the next value of of e.g. $\varepsilon = 0.55$, in order to speed up the process. This also has the associated benefit of ensuring that a particular mode is followed when the eigenvalues of two modes cross.

In order to improve the accuracy of the predictions presented here an extrapolation procedure is used. As the finite difference approximations to the governing equations and the boundary conditions are second order accurate we write

$$\lambda_n(\varepsilon) = \lambda_\infty(\varepsilon) + \frac{\lambda_1(\varepsilon)}{m_y^2} \tag{19}$$

and then use results at two different values of m_y to find the two corresponding values of $\lambda_\infty(\varepsilon)$ and $\lambda_1(\varepsilon)$ for each ε. Convergence for the first and third modes for the case $\alpha = 3$ is shown in Figure 7, using calculations carried out with $m_x = 240, m_y = 80$ and $m_x = 180, m_y = 60$. The relative errors clearly increase with mode number, but are of the order of 1% or less in the worst case at the highest resolution employed. Results for $\alpha = 1$ are somewhat more accurate.

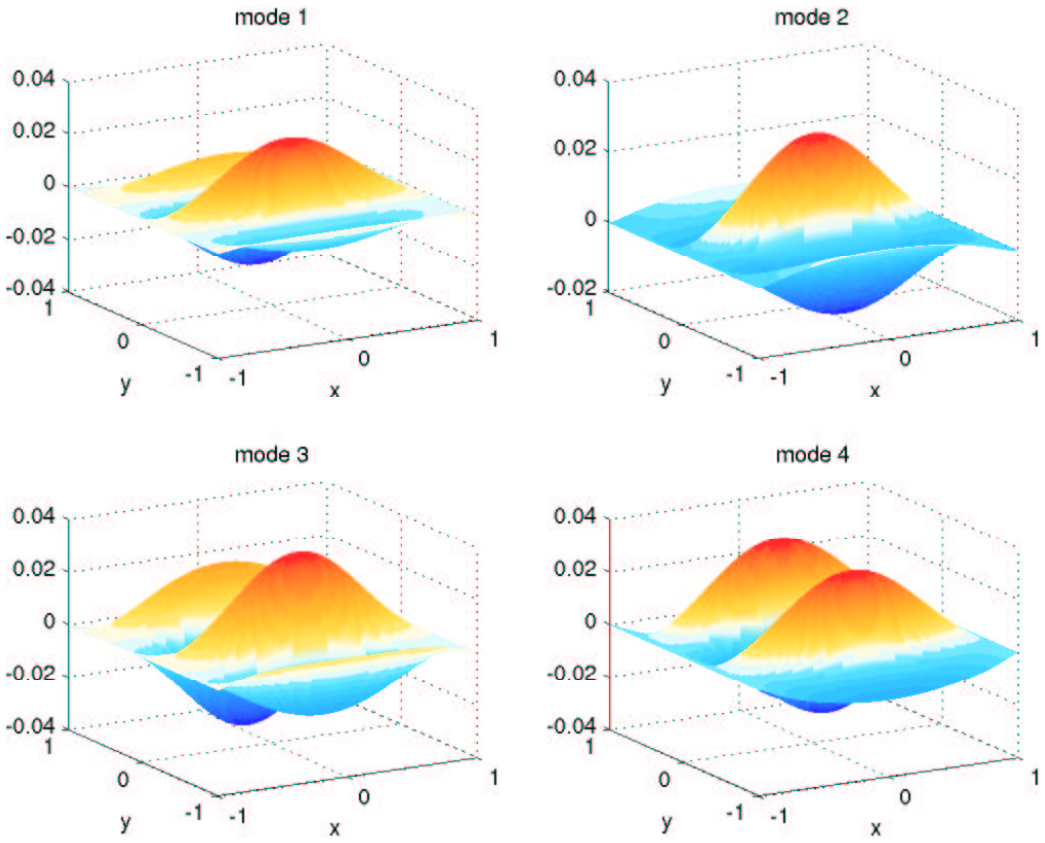

Figure 5: The eigenmodes corresponding to the four smallest positive eigenvalues λ for a square plate, i.e. $\alpha = 1$. The amplitude scale is arbitrary.

The variation of the eigenvalues with vertical amplitude is quite small, indicating that although large values of applied end-tension are needed to excite deformation, small changes from these values will lead to relatively large changes in amplitude.

Figure 8 shows the extrapolated eigenvalues λ_∞ as a function of the vertical amplitude ε for $\alpha = 1$. These extrapolated results were found using results calculated with $m_x = m_y = 90$ and $m_x = m_y = 120$. The modes clearly separate into two pairs, with the smaller eigenvalues of magnitude around 1200, while the larger eigenvalues are nearly twice as large. As mentioned earlier for each pair there is one mode that is odd in y while the other is even in y.

Figure 9, for $\alpha = 3$, shows results for λ_∞ similar to those displayed in Figure 8, determined as in Figure 7. The smallest eigenvalues are now significantly larger than those found for the square plate (nearly twice as big), indicating that greater tension is required to cause deformation in the elongated plate case. Although the eigenvalues for the two higher modes are also greater than for the square plate case, the difference between the values for the eigenvalues for the higher and lower modes is significantly reduced. It is possible that as $\alpha \to \infty$ the eigenvalues will continue to grow closer, or even cross, although this remains to be determined.

To see the relevance of these results for the BlueScope steel problem consider the following approximate data (Dr Andrew Dixon, private communication). Typical values for the thick-

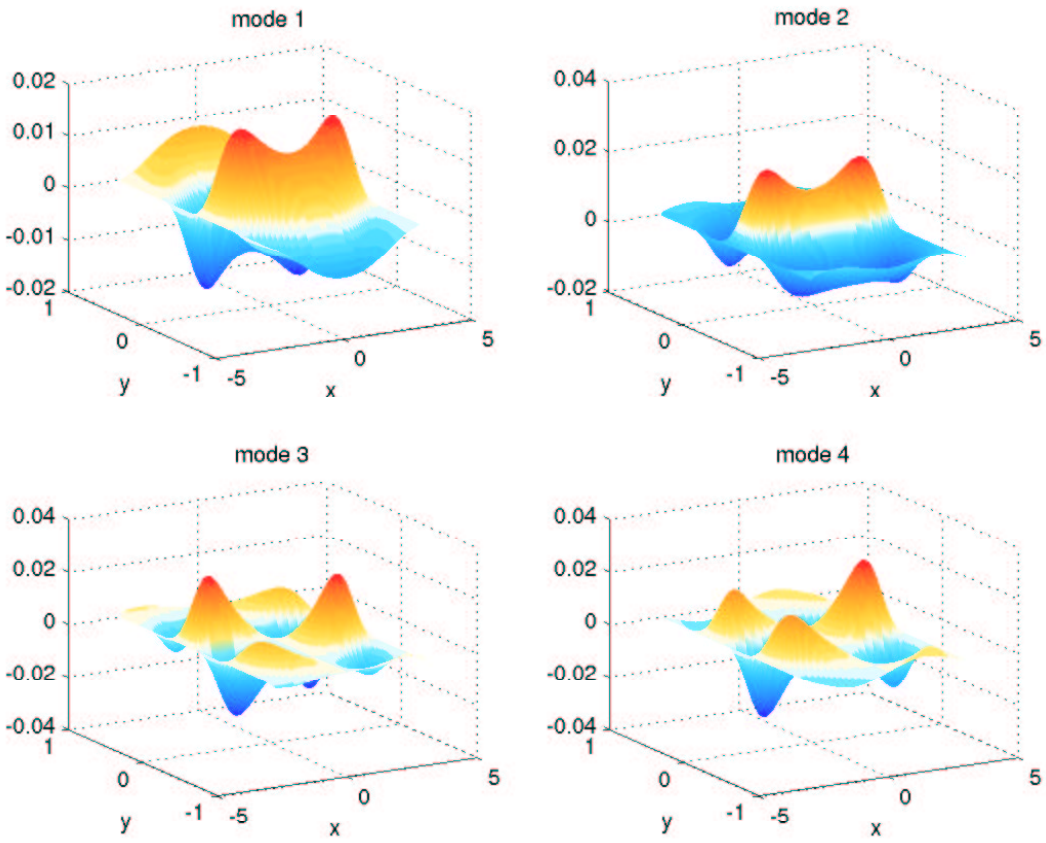

Figure 6: The eigenmodes corresponding to the four smallest positive eigenvalues λ for a rectangular plate with $\alpha = 3$. The amplitude scale is arbitrary.

ness and depth of the thin sheet steel are $h = 0.5$mm and $d = 0.5$m respectively. Young's modulus for steel has the value $E = 2 \times 10^{11}$ N/m^2 while typical applied end-stresses are of order of magnitude $N_0/h = 10^7$ N/m^2. See Table 1 for a list of approximate values of relevant material properties. Using these values in the relation (9) for λ gives $\lambda = O(500)$ in practice. This is much less than the critical values of over 2000 we calculate are needed for buckling. Thus significantly greater tensions would have to be applied in a perfectly symmetric situation as considered here to generate any significant distortion, as it appears the practical situation corresponds to large values of α. However, if there is any asymmetry in the applied forces, due for example to poor setup of equipment, it seems likely that deformation will arise at smaller applied tension. This implies that when wrinkles are observed in practice, they are likely to be due to roller misalignment, since our symmetric theory says tensions need to be four times the usual value to get wrinkling. However, the problem of asymmetry due to roller misalignment is beyond the scope of the present work and will be taken up in a subsequent paper where the parametric dependence of the eigenvalues on the degree of asymmetry will be explored.

If we assume for the moment that the applied end tension is sufficient to lead to plate deformation then further we can ask whether the amplitude of vertical deformation would be sufficient to cause plastic deformation. On geometric grounds it was proposed at MISG

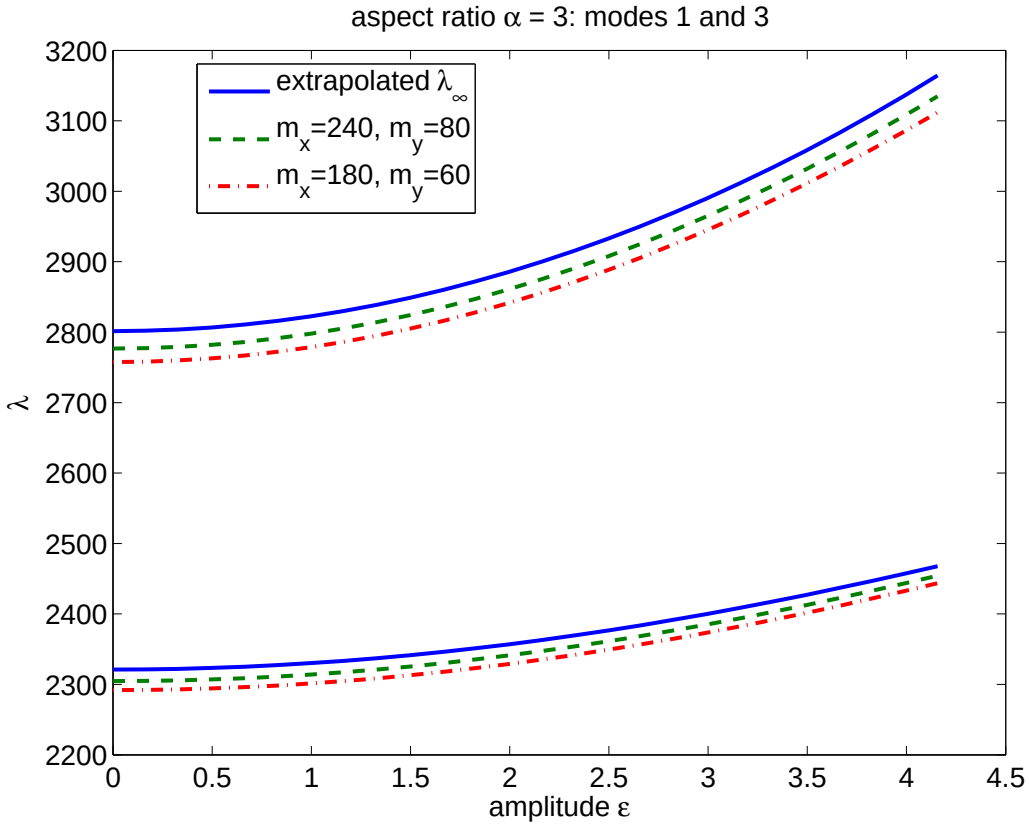

Figure 7: Convergence of the eigenvalues for $\alpha = 3$. The results for $m_x = 180$, $m_y = 60$ are shown dot-dashed ($- \cdot -$), the highest resolution results where $m_x = 240$, $m_y = 80$ with a dashed curve (- - -) and the extrapolated results λ_∞ as a solid line (—).

that curvature of the plate would be sufficient to cause plastic deformation if the radius of curvature, say r is less than the critical value $r_c = Eh/2\sigma_{\max} \approx 15$cm, where $\sigma_{\max}$ is the yield stress for steel (see Table 1). From Figures 5 and 6 we see that the wavelength in the y-direction is of order d/q with (approximately) $q = 3/4$ for modes 1 and 2, and $q = 1$ for modes 3 and 4, where q is a non-dimensional wavenumber. Using $q = 3/4$ and approximating the distortion of the plate as approximately sinusoidal, the ratio of deformation to wavelength in the y-direction corresponding to the critical radius of curvature r_c is approximately $1/20$. Therefore in dimensional variables for plastic deformation we require (recall non-dimensional w is scaled by d)

$$\frac{1}{20} \leq \frac{w}{\text{wavelength}} = q\sqrt{N_0/Eh}\,\varepsilon = \frac{3}{4}\frac{h}{d}\sqrt{\frac{\lambda}{12(1-\nu^2)}}\,\varepsilon\,, \tag{20}$$

and we find that, using the same approximate data as above,

$$\lambda\,\varepsilon^2 \geq 6 \times 10^4. \tag{21}$$

For example, in Figure 9, where $\lambda \approx 2000$ for the lower modes, we require $\varepsilon \approx 5$ to allow for

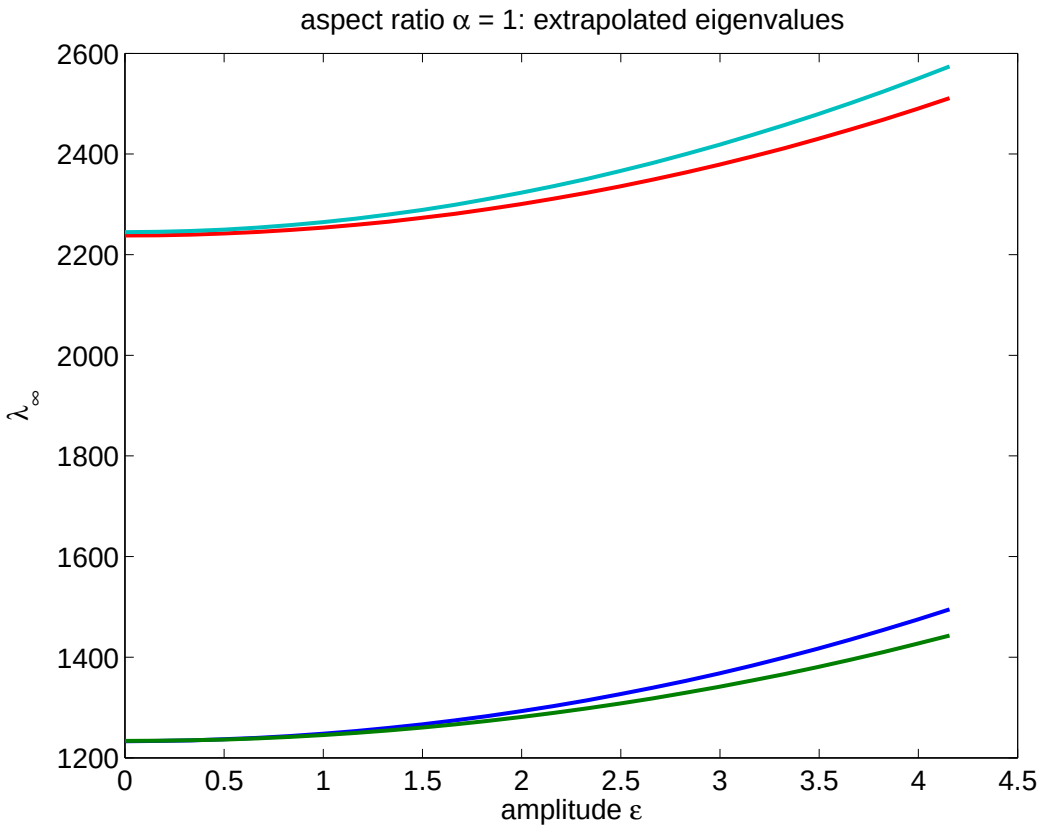

Figure 8: The four smallest positive eigenvalues λ_∞ for a square plate ($\alpha = 1$) as a function of the maximum vertical deformation ε. The eigenvalues are determined using the extrapolation procedure described in the text.

plastic deformation and so provide permanent distortion. This corresponds to a dimensional amplitude of

$$w = \varepsilon d\sqrt{\frac{N_0}{Eh}} = \frac{\varepsilon}{2}\sqrt{\frac{10^6}{2\times 10^{11}}} \approx 20 \text{ mm} . \tag{22}$$

Once such a transverse buckle has been created near the roller, we hypothesise that it undergoes a process of *ironing-in*, thus creating a permanent wrinkle at the roller. This process is discussed further in section 7.

5 An energy method

Paper [2] studied the wrinkling of a thin elastic sheet under tension, far from onset, using the principle of inextensibility to provide a lateral compression, and a Lagrangian energy development. They looked for periodic solutions to the Euler-Lagrange equations, and solved

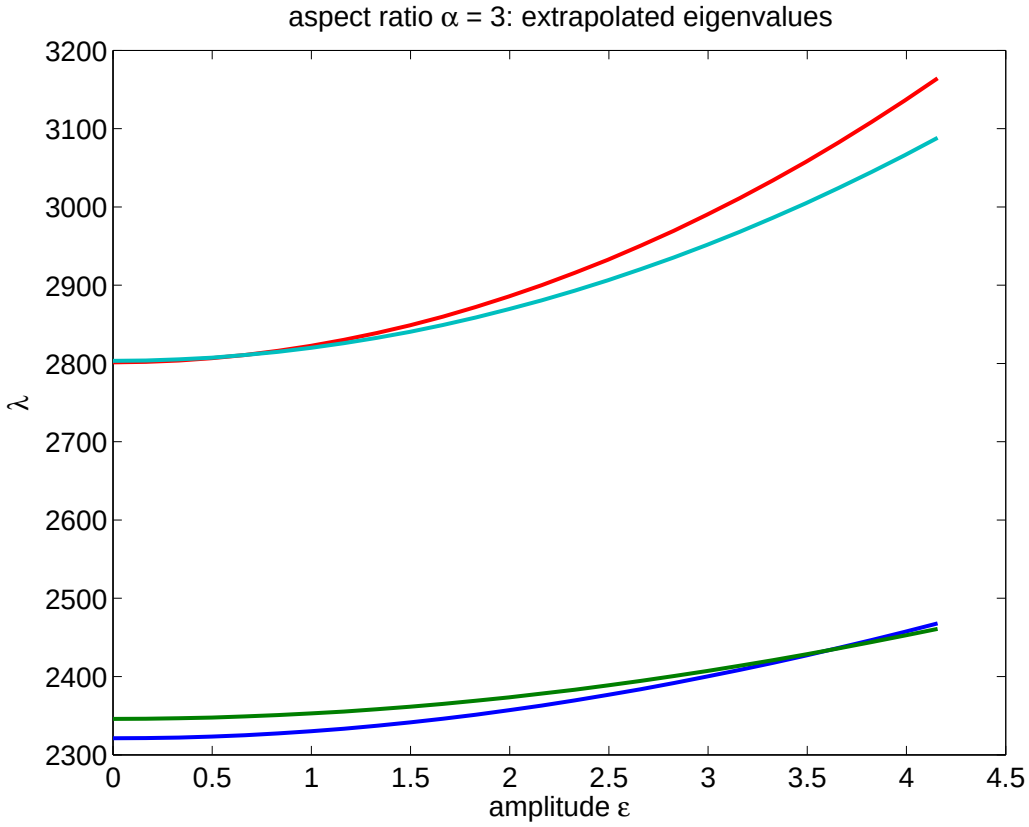

Figure 9: The four smallest positive eigenvalues λ_∞ for a rectangular plate ($\alpha = 3$) as a function of the maximum vertical deformation ε. The eigenvalues are determined using the extrapolation procedure described in the text.

the resulting Sturm-Liouville problem to find the expressions

$$L = \frac{\sqrt{4\pi\ell h}}{[3(1-\nu^2)\gamma]^{\frac{1}{4}}}, \quad a = \sqrt{2\nu\ell h}\left[\frac{16\gamma}{3\pi^2(1-\nu^2)}\right]^{\frac{1}{4}}, \tag{23}$$

for the wavelength L and amplitude a of the wrinkles, where the other symbols used here are as defined in Table 1. Using $\ell \approx 10$m gives $a \approx 3$mm and $L \approx 2$m.

These are quite different results to those of the previous section. The analysis of [2] does not consider the possibility that the steel does not buckle under smaller tensions - it assumes that the lateral compression caused by the applied tension is matched by bending energy across the sheet. That is, no bifurcation phenomenon is considered, and the sheet is assumed to always buckle. The question addressed is how much it buckles, if energy is conserved. Such an analysis might be considered to be more relevant in the presence of asymmetries, like small misalignments of the rollers, which would reduce the critical parameter value at which buckling occurs.

line speed	3 m/s
distance between rollers	$2\ell \approx$10–20 m
roller radius	$R = 25 - 30$cm
crown height of rollers	0.1 mm
roll location accuracy	1 mm
angle of misalignment of rollers	up to 0.06°
steel strip thickness	$h \approx 0.3$mm
steel strip width	$2d \approx 0.5$m
Young's Modulus	$E \approx 2 \times 10^{11}$Pa
Poisson's ratio for steel	$\nu_{\text{steel}} \approx 0.28$
Poisson's ratio for paper	$\nu_{\text{paper}} \approx 0.01$
flexural rigidity of steel	$D \equiv Eh^3/(12(1-\nu^2)) \approx 0.49$N.m
line tension	$N_0/h = \sigma \approx 10$MPa
longitudinal stretching strain	$\gamma \equiv N_0/(Eh)$
yield stress for steel	$\sigma_{\max} \approx 200$MPa
coefficient of friction for steel	$\mu \approx 0.1$
areal density of steel	$\varrho \approx 2\text{kg/m}^2$

Table 1: Material properties used for rolled steel

6 Waves on steel

The group also considered the speeds of bending waves and compressional waves on and in steel, compared with the typical operational linespeeds of the steel over the rollers. Bending waves are governed by the balance

$$D\frac{\partial^4 w}{\partial x^4} = -\varrho\frac{\partial^2 w}{\partial t^2} \tag{24}$$

where ϱ is the areal density, about 2 kg/m^2. Setting $w = \exp[i(kx - \omega t)]$ where $\omega = 1/\tau$ and τ is the period of the waves, gives

$$k^4 D = \omega^2 \varrho \;\Rightarrow\; \tau = L^2\sqrt{\frac{\varrho}{D}} \tag{25}$$

and hence the wavespeed is $c = \frac{L}{\tau} \approx \frac{1}{L}$, since $D \approx \varrho$. Hence for wavespeed to be greater than the linespeed of 3 m/s, the wavelength needs to be shorter than 1/3 m. These shorter bending waves can propagate upstream against the flow of the steel. In particular, so can the waves predicted by the theory of [2] discussed in the previous section.

Tensional wave speed may be estimated by balancing

$$N_0\frac{\partial^2 w}{\partial x^2} \sim \varrho\frac{\partial^2 w}{\partial t^2}, \tag{26}$$

which gives the wavespeed squared as $c^2 \sim \frac{N_0}{\varrho}$, which leads to $c \approx 40$m/s, which is much faster than linespeed. Hence tension changes propagate rapidly compared with linespeed, and linespeed may be ignored when calculating stress fields as in the first section.

7 Ironing in the wrinkles

Here we consider whether the pressure on the steel as it goes around a roller is sufficient to iron-in a wrinkle. To iron the wrinkle in, yield stress needs to be exceeded in the steel as it passes over the roller. The coiling pressure gives a measure of the downward pressure that is applied to a wrinkle. This is

$$P = \sigma h/R \approx 0.01 \text{ MPa} , \tag{27}$$

which is taken to act towards the roller axis as a force per unit length across the roller and which also gives rise to a total uniform loading Pb towards the roller axis acting on the wrinkle. The numerical value in equation (27) is found using the values given in Table 1.

First we use a very simplified model of the deformation shown in Figure 10(a) in order to approximate the relation between the height a, the width of the wrinkle b and the contact distance δ. We consider a strip of plate of unit width in the direction aligned with the roller axis and approximate the deflection $w(y)$ given by the triangular function shown in Figure 10(b). Assuming symmetry of this triangular shape, the forces acting on the section AB of the plate are shown in Figure 10(c). $H = \mu P\delta$ is the force due to the friction between the roller and the section of the plate fully in contact with the roller.

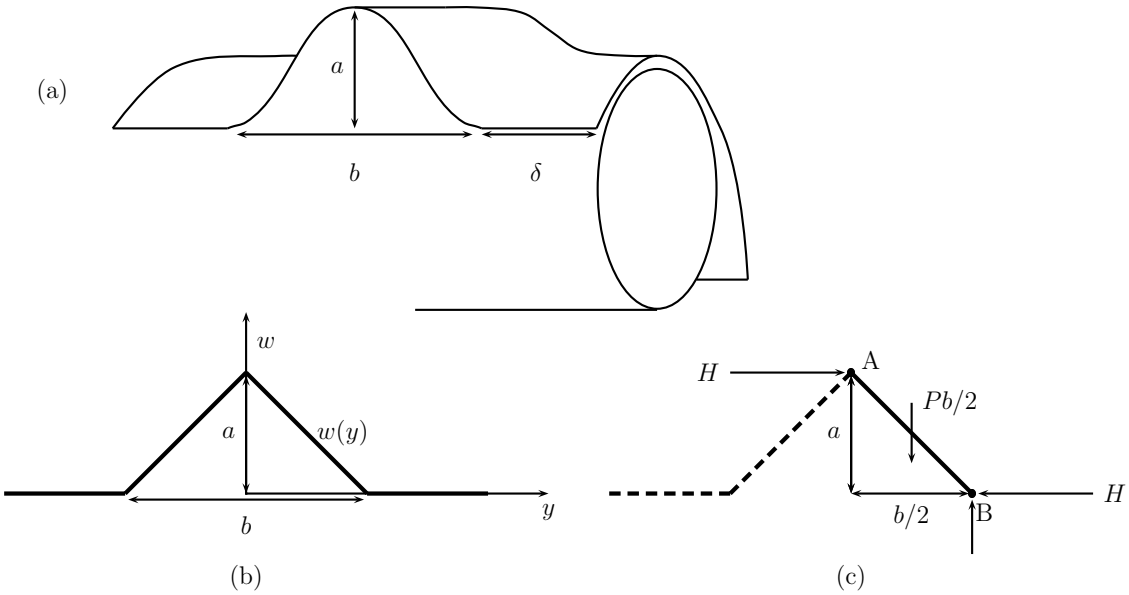

Figure 10: (a) Sketch of a wrinkle wrapping around a roller with (b) the approximate deflection $w(y)$ and (c) the corresponding free body diagram.

Considering the moment equilibrium about the point B we obtain $Ha = Pb^2/8$. After rearrangement $H = \mu P\delta = Pb^2/8a$, so that, with the friction coefficient $\mu = 0.1$, $\delta = 5b^2/4a$ which provides an approximate relation between a, b and δ. We also have the relation $2\delta + b = 2d$.

Finally we require the critical lateral force per unit length F_c that is required to cause this buckle in a plate. We will approximate this value by using the following result on plate

buckling from [12], p.352,

$$\frac{m^2 F_c}{\pi^2 b^2 D} = \left(\frac{m^2}{b^2} + \frac{n^2}{4\ell^2} \right)^2$$

where m is the lateral wavenumber, n is the longitudinal wavenumber, and 2ℓ is the length of the plate. Taking $n = 0$ and $m = 1$ gives the critical lateral force per unit length for buckling as $F_c = \frac{\pi^2 D}{b^2}$.

For friction to provide enough lateral force to sustain the wrinkle of amplitude a as the sheet passes over the free roller we require $H > F_c$, which implies

$$H = \mu P \delta \geqslant F_c = \frac{\pi^2 D}{b^2} \ . \tag{28}$$

Substituting for δ we obtain the cubic equation for the value of b at the critical buckling load

$$b^2(2d - b) = \frac{2\pi^2 D}{\mu P}, \tag{29}$$

or $b^2(0.5 - b) \approx 0.01$, by using the numerical value of P given by equation (27) and the values of μ, d and D in Table 1. The cubic equation for b has two positive roots, $b \approx 0.18$m and $b \approx 0.45$m, where the larger value is near to the full strip width. For b between these two limits, friction can hold against the critical lateral bending force, and the wrinkle is ironed-in as it passes over the roller. Hence if the contact length between roller and steel is in the range 160mm $\geqslant \delta \geqslant$ 25mm, there is enough friction to hold the steel edges in place and prevent the wrinkle from disappearing. The smallest wrinkle width that can be supported according to this model is about $b = 175$mm across. This is significantly larger than the measurement shown in Figure 1. However, it appears that the pressure induced by the *longitudinal* stress at the wrinkle as it wraps around the roller gives a much larger value for P than that used here, so providing a much smaller critical value for the smallest wrinkle width b that can be supported (see [4]) and correspondingly a value more closely in accord with observations.

The corresponding amplitude of the wrinkle for this range of b (or equivalently δ) can be estimated. Using $H = \mu P \delta = P b^2 / 8a$, we have

$$a = b^2/(8\mu\delta) = b^2/(4\mu(2d - b)) \ . \tag{30}$$

Therefore, according to this balance between downward pressure and friction the smallest wrinkle amplitude a that can be supported is about 250mm when $b = 180$mm. The amplitude a increases monotonically as b is increased. This large value of the amplitude is clearly physically unrealistic, but again is very significantly reduced if the enhanced pressure proposed by [4] is used.

8 Conclusions

The formation of longitudinal wrinkles in thin steel sheet can be identified with the modes of deformation occurring when a thin plate is placed under sufficiently large longitudinal tension. Solving the biharmonic equation describing the stress distribution in a rectangular plate, with free transverse edges and and applied stress at the ends corresponding to that for convex rollers, shows that a local compressive in-plane stress is produced transverse to the plate. In response to this compressive stress wrinkles aligned in the longitudinal direction may arise,

depending on the magnitude of the applied tension. However, the critical stress for wrinkles to initiate is about four times the stress we predict in the BlueScope Steel setup, suggesting that any longitudinal wrinkles observed are due to asymmetries from, say, misalignment of rollers or damaged roller surfaces.

The zeroth order approximation to the full von Kármán plate bending equations gives rise to a linear eigenvalue problem for the applied longitudinal tension, with any particular eigenvalue giving the critical (non-dimensionalised) applied force above which the corresponding eigenmode of vertical deformation will arise. However, this linearised problem does not give any information about the amplitude of vertical deformation. In order to determine the amplitude, the nonlinear von Kármán equations must be iterated. This process results in generally small changes in the stress distribution in the plate and the form of the corresponding modes of vertical deformation as compared to the linear case.

As the eigenvalues are found to vary quite slowly with the vertical amplitude, the physical conclusion is that if the applied tension is sufficient to excite a particular mode, then the amplitude of deformation may be quite significant for small changes in applied tension above critical. The expression (20) indicates that local *plastic* deformation may be observed if the longitudinal tension is sufficient to cause wrinkling distortions. In particular, this is expected to occur at the point where maximum deformation is observed. This will occur at the mid-line of the plate for the low-order mode even in y (mode 2 in Figures 5 and 6).

According to the model used in section 7, only quite wide, large amplitude wrinkles can be ironed-in at the roller. In order to provide a mechanism for the formation of unwanted permanent distortions of sheet metal as observed in practice in some cases, significantly greater local pressure at the wrinkle is required. One proposed mechanism for this is the enhanced longitudinal stress at the wrinkle as it passes over the roller, as discussed in [4].

Acknowledgements

The moderators would like to thank the MISG participants who contributed so much to this work: Bob Anderssen, Steve Barry, John Cogill, Grant Cox, Jonathan Crook, Bronwyn Hayek, Roslyn Hickson, Da Eun Jeon, Scott McCue, Robert McKibbin, Steve Taylor and Peter Tritscher. We also thank the BlueScope steel representatives, Andrew Dixon, Daniel Yuen and Maria Cozijnsen for their participation, expertise, and strong support in all phases of the project.

References

[1] Baglama, J. (2007) `ahbeigs.m` available at http://www.math.uri.edu/~jbaglama/ (see also the MATHWORKS site http://www.mathworks.com/matlabcentral/fileexchange/).

[2] Cerda, E. & Mahadevan, L. (2003) Geometry and physics of wrinkling, *Phys. Rev. Lett.*, **90**, 074302-1 – 0704302-4.

[3] Chien, C.-S., Gong, S.-Y. & Mei, Z. (2000) Mode jumping in the von Kármán equations, *SIAM J. Sci. Comput.*, **22**, 1354–1385.

[4] Dixon, A. & Yuen, W.Y.D. (2007) Crease formation in the processing of thin web material, to appear in *Proceedings of the 5th Australasian Congress on Applied Mechanics, ACAM 2007*, 10–12 December, Brisbane, Australia. 6pp.

[5] Dossou, K. & Pierre, R. (2003) A Newton-GMRES approach for the analysis of the postbuckling behaviour of the solutions of the von Kármán equations, *SIAM J. Sci. Comput.*, **24**, 1994–2012.

[6] Fischer, F.D., Rammerstorfer, Friedl, N. & Wieser, W. (2000) Buckling phenomena related to rolling and levelling of sheet metal, *Int. J. Mech. Sci*, **42**, 1887–1910.

[7] Hashimoto, H. (2007) Prediction model of paper-web wrinkling and some numerical calculation examples with experimental verifications, *Microsystem Technologies-Micro and Nanosystems-Information Storage and Processing Systems*, **13**, 933–941.

[8] Mansfield, E.H. (1989) *The bending and stretching of plates*, 2nd edition, Cambridge University Press, New York.

[9] Muradova, A.D. (2005) Numerical techniques for linear and nonlinear eigenvalue problems in the theory of elasticity, *ANZIAM J.* **46 (E)**, C426–C438.

[10] Schaeffer, D.G. & Golubitsky, M. (1979) Boundary conditions and mode jumping in the buckling of a rectangular plate, *Commun. Math. Phys.*, **69**, 209–236.

[11] Timoshenko, S.P. & Woinowsky-Krieger, S. (1959) *Theory of plates and shells* 2nd edition. McGraw-Hill Book Company, New York.

[12] Timoshenko, S.P. & Gere, J.M. (1961) *Theory of elastic stability*, 2nd edition, McGraw–Hill, New York.

[13] Wong, Y.W. & Pellegrino, S. (2006) Wrinkled membranes I: experiments, *J. Mech. Materials Struct.*, **1**, 3–25.

[14] Wong, Y.W. & Pellegrino, S. (2006) Wrinkled membranes II: analytical models, *J. Mech. Materials Struct.*, **1**, 27–61.

[15] Wong, Y.W. & Pellegrino, S. (2006) Wrinkled membranes I: numerical simulations, *J. Mech. Materials Struct.*, **1**, 63–95.